Efficient Solution of the Combined-Field Integral Equation with the Parallel Multilevel Fast Multipole Algorithm

Levent Gürel[1,2] and Özgür Ergül[1,2]

[1]*Department of Electrical and Electronics Engineering*
[2]*Computational Electromagnetics Research Center (BiLCEM)*
Bilkent University, TR-06800, Bilkent, Ankara, Turkey
lgurel@bilkent.edu.tr, ergul@ee.bilkent.edu.tr

***Abstract*— We present fast and accurate solutions of large-scale scattering problems formulated with the combined-field integral equation. Using the multilevel fast multipole algorithm (MLFMA) parallelized on a cluster of computers, we easily solve scattering problems that are discretized with tens of millions of unknowns. For the efficient parallelization of MLFMA, we propose a hierarchical partitioning scheme based on distributing the multilevel tree among the processors with an improved load-balancing. The accuracy of the solutions is demonstrated on scattering problems involving spheres of various radii from 80λ to 110λ. In addition to canonical problems, we also present the solution of real-life problems involving complicated targets with large dimensions.**

I. Introduction

For the numerical solution of scattering problems in electromagnetics, surface integral equations provide accurate results when they are discretized appropriately by using small elements with respect to wavelength [1]. When the scatterer involves closed surfaces, the combined-field integral equation (CFIE) is usually preferred to formulate the problem, since it is free of the internal resonances [2] and provides well-conditioned matrix equations compared to the electric-field integral equation (EFIE) and the magnetic-field integral equation [3]–[5]. Simultaneous discretizations of the scatterer and CFIE lead to dense matrix equations, which can be solved iteratively with the accelerated matrix-vector multiplications (MVMs) by the multilevel fast multipole algorithm (MLFMA) [6]. On the other hand, accurate solutions of many real-life problems require discretizations with millions of unknowns. To solve these large problems, it is helpful to increase computational resources by assembling parallel computing platforms and at the same time by parallelizing the solvers. Recently, there have been many efforts to develop parallel implementations of MLFMA running on clusters of computers connected via fast networks. Thanks to these efforts, it has become possible to solve 20–30 million unknowns on relatively inexpensive computing platforms [7]–[12].

In this paper, we present our efforts to develop a sophisticated simulation environment based on parallel MLFMA for the solution of large-scale scattering problems formulated by CFIE. Due to its complicated structure, parallelization of MLFMA is not trivial. Simple parallelization strategies usually fail to provide efficient solutions because of the communications between the processors and the unavoidable duplication of some of the computations over multiple processors. Our approach involves load-balancing and partitioning techniques to distribute the tasks equally among the processors. We propose a hierarchical partitioning scheme based on distributing the multilevel tree among the processors with an improved load-balancing to achieve an efficient parallelization of MLFMA. We demonstrate the accuracy and efficiency of our implementations on scattering problems involving spheres of various radii up to 110λ discretized with 41,883,638 unknowns. We also demonstrate the effectiveness of our simulation environment by presenting examples on scattering problems involving complicated targets with large numbers of unknowns.

II. Multilevel Fast Multipole Algorithm

For the solution of scattering problems involving three-dimensional conducting bodies with closed surfaces, discretization of CFIE leads to $N \times N$ dense matrix equations

$$\sum_{n=1}^{N} Z_{mn} a_n = v_m, \qquad m = 1, 2, ..., N, \tag{1}$$

where a_n represents the unknown coefficients of the basis functions $\boldsymbol{b}_n(\boldsymbol{r})$ for $n = 1, 2, ..., N$ to expand the surface current density, i.e.,

$$\boldsymbol{J}(\boldsymbol{r}) \approx \sum_{n=1}^{N} a_n \boldsymbol{b}_n(\boldsymbol{r}). \tag{2}$$

In (1), Z_{mn} represents the matrix elements derived as

$$Z_{mn} = \alpha_m Z_{mn}^E + (1 - \alpha_m) Z_{mn}^M, \tag{3}$$

where

$$Z_{mn}^E = -ik \int_{S_m} d\boldsymbol{r} \boldsymbol{t}_m(\boldsymbol{r}) \cdot \int_{S_n} d\boldsymbol{r'} \boldsymbol{b}_n(\boldsymbol{r'}) g(\boldsymbol{r}, \boldsymbol{r'}) + \frac{i}{k} \int_{S_m} d\boldsymbol{r} \boldsymbol{t}_m(\boldsymbol{r}) \cdot \int_{S_n} d\boldsymbol{r'} \nabla \nabla' g(\boldsymbol{r}, \boldsymbol{r'}) \cdot \boldsymbol{b}_n(\boldsymbol{r'}) \tag{4}$$

978-1-4244-1606-6/07/$25.00 ©2007 IEEE

and

$$Z_{mn}^{M} = \int_{S_m} d\boldsymbol{r}\boldsymbol{t}_m(\boldsymbol{r}) \cdot \boldsymbol{b}_n(\boldsymbol{r}) - \int_{S_m} d\boldsymbol{r}\boldsymbol{t}_m(\boldsymbol{r}) \cdot \hat{\boldsymbol{n}}(\boldsymbol{r}) \times \int_{S_n} d\boldsymbol{r'}\boldsymbol{b}_n(\boldsymbol{r'}) \times \nabla' g(\boldsymbol{r}, \boldsymbol{r'}) \tag{5}$$

are the contributions of EFIE and MFIE, respectively. In (4) and (5), $\boldsymbol{t}_m(\boldsymbol{r})$ represents the mth testing function, $\hat{\boldsymbol{n}}(\boldsymbol{r})$ is the unit normal vector at the testing point $\boldsymbol{r}$,

$$g(\boldsymbol{r}, \boldsymbol{r'}) = \frac{e^{ikR}}{4\pi R} \qquad \left(R = |\boldsymbol{r} - \boldsymbol{r'}|\right) \tag{6}$$

denotes the free-space Green's function in phasor notation with the $\exp(-iwt)$ convention, and $k = w\sqrt{\mu\epsilon}$ is the wavenumber. Similarly, elements of the right-hand-side vector in (1) can be written as

$$v_m = \frac{\alpha_m}{\eta} \int_{S_m} d\boldsymbol{r}\boldsymbol{t}_m(\boldsymbol{r}) \cdot \boldsymbol{E}^{inc}(\boldsymbol{r}) + (1 - \alpha_m) \int_{S_m} d\boldsymbol{r}\boldsymbol{t}_m(\boldsymbol{r}) \cdot \hat{\boldsymbol{n}}(\boldsymbol{r}) \times \boldsymbol{H}^{inc}(\boldsymbol{r}), \tag{7}$$

where $\boldsymbol{E}^{inc}(\boldsymbol{r})$ and $\boldsymbol{H}^{inc}(\boldsymbol{r})$ are the incident electric and magnetic fields, and $\eta = \sqrt{\mu/\epsilon}$ is the characteristic impedance of free space.

In this paper, surfaces are discretized by using small triangles, on which Rao-Wilton-Glisson (RWG) [13] functions are defined. We use the same set of RWG functions as the basis and testing functions according to a Galerkin scheme. The matrix equation in (1) can be solved iteratively, where the MVMs are accelerated by MLFMA. For an $N \times N$ dense matrix equation, MLFMA reduces the complexity of the MVMs from $O(N^2)$ to $O(N \log N)$. This is achieved by considering the matrix elements as the electromagnetic interactions and calculating the far-field interactions in group-by-group manner. A tree structure is constructed by including the scatterer in a cubic box and recursively dividing the computational domain into subboxes (clusters). Then, MLFMA splits the MVMs as

$$\bar{\boldsymbol{Z}} \cdot \boldsymbol{x} = \bar{\boldsymbol{Z}}_{NF} \cdot \boldsymbol{x} + \bar{\boldsymbol{Z}}_{FF} \cdot \boldsymbol{x}, \tag{8}$$

where the near-field interactions denoted by $\bar{\boldsymbol{Z}}_{NF}$ are calculated directly and stored in memory. For these interactions, the integrals in (4) and (5) on the supports of the basis and testing functions (S_n and S_m) are evaluated accurately by employing Gaussian quadrature rules, adaptive integration methods, and singularity extraction techniques [14]–[19]. The rest of the interactions, i.e., the far-field interactions denoted by $\bar{\boldsymbol{Z}}_{FF}$, are computed approximately via three main stages performed on the multilevel tree [20]:

1) Aggregation: Radiated fields at the centers of the clusters are calculated from the bottom of the tree structure to the highest level. Oscillatory nature of the Helmholtz solutions requires that the sampling rate for the fields depend on cluster size as measured by the wavelength [21]. During the aggregation stage, we employ local Lagrange interpolation to match the different sampling rates of the consecutive levels [22].
2) Translation: Radiated fields at the centers of the clusters are translated into incoming fields for other clusters.
3) Disaggregation: The total incoming fields at the centers of the clusters are calculated from the top of the tree structure to the lowest level. At the lowest level, the incoming fields are received by the testing functions. During the disaggregation stage, we employ local Lagrange anterpolation (transpose interpolation) method to match the different sampling rates of the consecutive levels [22],[23].

The tree structure of MLFMA includes $L = O(\log N)$ levels. At level l from 1 to L, the number of nonempty boxes (clusters) is N_l, where $N_1 = O(N)$ and $N_L = O(1)$. In our implementations, radiated and incoming fields of the clusters are sampled uniformly in the ϕ direction, while we use the Gauss-Legendre quadrature in the θ direction. There are a total of $S_l = (T_l + 1) \times (2T_l + 2)$ samples required for a cluster in level l, where T_l is the truncation number determined by the excess bandwidth formula as [21]

$$T_l \approx 1.73ka_l + 2.16(d_0)^{2/3}(ka_l)^{1/3}. \tag{9}$$

In (9), a_l is the cluster size at level l and d_0 is the desired digits of accuracy. We note that $S_1 = O(1)$ and $S_L = O(N)$. Considering the number of clusters (N_l) and the samples of the fields (S_l), all levels of MLFMA have equal importance with $N_l S_l = O(N)$ complexity in terms of processing time and memory.

III. Parallelization of MLFMA

Because of its complicated structure, parallelization of MLFMA is not trivial and simple parallelization strategies usually fail to provide efficient solutions. For the parallelization of MLFMA, the main task is to distribute the tree structure among the processors. Since all levels of MLFMA have equal importance with $O(N)$ complexity, an efficient parallelization of MLFMA should attempt to obtain the best partitioning for each level.

A. Partitioning of the Tree Structure

For the efficient parallelization of MLFMA, we use a hierarchical partitioning scheme, where both the clusters and and the samples of the fields are partitioned for all levels. This strategy is illustrated on a 4-level tree structure in Fig. 1, where the levels are represented by two-dimensional rectangular boxes including various numbers of clusters (horizontal dimension) and samples of the fields (vertical dimension). Each level is partitioned among 16 processors. Using the hierarchical strategy, we adjust the numbers of partitions appropriately by considering the numbers of clusters and the samples of the fields. As depicted in Fig. 1, the clusters in the lowest level are distributed among all processors without any partitioning of the fields. As we proceed to the higher levels, however, the numbers of partitions for the clusters and the fields are

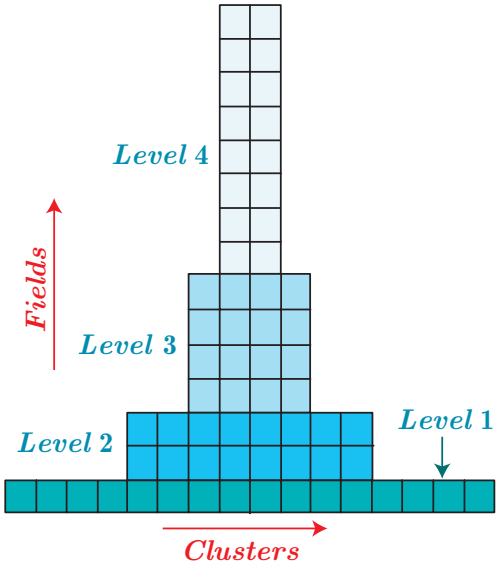

Fig. 1. Hierarchical partitioning of a 4-level tree structure.

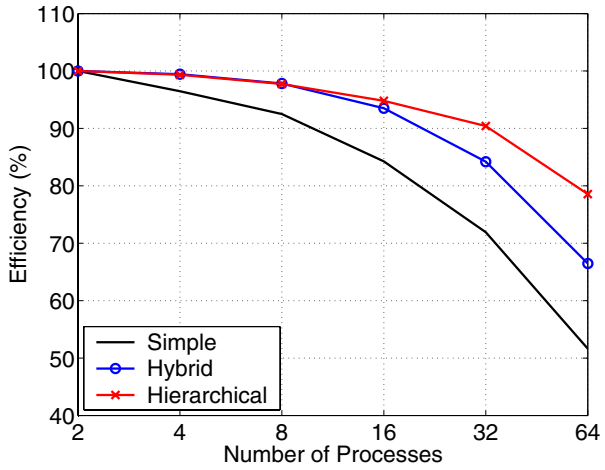

Fig. 2. Parallelization efficiency for the solution of a scattering problem involving a sphere of radius 30λ discretized with 3,319,524 unknowns.

systematically decreased and increased, respectively. In this way, the computations for all levels are distributed among the processors with improved load-balancing.

To demonstrate the improved efficiency of the hierarchical parallelization, we present the solution of a scattering problem involving a conducting sphere of radius 30λ discretized with 3,319,524 unknowns. The sphere is illuminated by a plane wave and 7-level MLFMA is used to solve the problem on a cluster of 2.33 GHz quad-core Intel Xeon processors connected via an Infiniband network. Fig. 2 depicts the efficiency when the solution is parallelized into 2, 4, 8, 16, 32, and 64 processors. The parallelization efficiency is defined as

$$\varepsilon_p = \frac{2T_2}{pT_p}, \tag{10}$$

where T_p is the processing time of the solution with p processors. In addition to the hierarchical parallelization, we

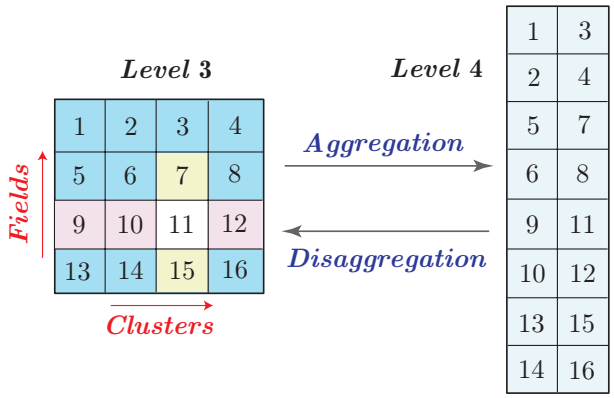

Fig. 3. Partitioning and processor assignments for the 3rd and 4th levels of the tree structure in Fig. 1.

consider simple and hybrid partitioning schemes. In the simple partitioning scheme, clusters in all levels are distributed among the processors and each cluster at any level is assigned to a single processor [11]. In the hybrid partitioning scheme, however, different strategies are applied for the lower and the higher levels of the tree structure; depending on the level, only the clusters or the samples of the fields are distributed among the processors [10]. All parallelization strategies are optimized via load-balancing algorithms. Fig. 2 shows that the hierarchical parallelization offers higher efficiency compared to both simple and hybrid parallelization schemes. Using 64 processors and the hierarchical parallelization, the efficiency is 80%, which corresponds to 25-fold speed-up compared to the two-processor solution.

B. Communications in Parallel MLFMA

In parallel MLFMA, processors need to communicate with each other to transfer data, which must be organized carefully. Using the hierarchical partitioning scheme, there are three different types of communications required in the MVMs. As an example, we consider the third level of the tree structure in Fig. 1, where both the clusters and the samples of the fields are divided into 4 partitions. Fig. 3 depicts the processor assignments from $p = 1$ to $p = 16$.

1) Communications for translations: Due to the partitioning of the clusters, some of the translations are related to basis and testing clusters that are located in different processors. Therefore, one-to-one communications are required between processors to perform these translations. As an example, processor 11 communicates with processors 9, 10, and 12 in Fig. 3.
2) Communications for interpolation and anterpolation operations: Due to the partitioning of the samples of the fields, interpolation operations during the aggregation stage require communications between the processors [10]. In general, each processor needs samples that are located in other processors. Partitioning the samples only along θ direction, these communications are mainly required between the processors located "close to each other." As an example, processor 11 communicates with

TABLE I

TREE STRUCTURES FOR LARGE SPHERE PROBLEMS

Diameter	Unknowns	Levels	Clusters	Cluster Size	T_l
120λ	13,278,096	8	1,510,758	0.235λ–30λ	6–346
160λ	23,405,664	9	5,769,254	0.156λ–40λ	5–457
192λ	33,791,232	9	5,904,951	0.188λ–48λ	6–546
220λ	41,883,648	9	5,975,507	0.215λ–55λ	6–623

TABLE II

SOLUTIONS OF LARGE SPHERE PROBLEMS WITH MLFMA PARALLELIZED INTO 16 PROCESSES

Diameter	Setup (min.)	Iterations	MVM (sec.)	Solution (min.)
120λ	114	15	131	67
160λ	104	17	307	178
192λ	205	21	406	289
220λ	313	19	467	314

processors 7 and 15 in Fig. 3. Similar to the interpolations in the aggregation stage, some of the data produced by the anterpolation operations during the disaggregation stage should be sent to other processors via one-to-one communications.

3) Communications to modify the partitioning: Using the hierarchical parallelization strategy, the partitioning should be changed between levels during the aggregation and disaggregation stages. This is achieved by exchanging data between pairs of processors. For example, following the aggregation operations from level 3 to level 4 in Fig. 3, processor 11 exchanges data with processor 12. Similarly, data exchanges are required following the disaggregation operations from level 4 to level 3.

Finally, to improve the efficiency of the parallelization, we use nonblocking send and receive operations of message passing interface (MPI) to transfer the data in all communications.

IV. RESULTS

By constructing a sophisticated simulation environment based on parallel MLFMA, we are able to solve scattering problems discretized with tens of millions of unknowns. As an example, we present the solution of large scattering problems involving spheres of radii 60λ, 80λ, 96λ, and 110λ, which are discretized with 13,278,096, 23,405,664, 33,791,232, and 41,883,648 unknowns, respectively. For each problem, we construct the multilevel tree structure by using a top-down strategy, where the target is enclosed in the smallest possible cubic box and the computational domain is recursively divided into subboxes until the size of the clusters is in the range from 0.15λ to 0.30λ. The details of the tree structures are listed in Table I, including the number of levels, total number of clusters, size of the clusters, and the truncation number T_l in the lowest and the highest levels involving translations. Spheres are illuminated by a plane wave propagating in the $-x$ direction and the scattering problems are solved by an MLFMA implementation parallelized into 16 processes running on a cluster of 2.33 GHz quad-core Intel Xeon processors connected via an Infiniband network. In MLFMA, near-field and far-field interactions are calculated with 1% error. Details of the solutions are presented in Table II, where we list the setup time, number of BiCGStab iterations for 0.001 residual error, processing time for each MVM, and the time required for the iterative solution. We observe that the largest problem with 41,883,648 unknowns is solved in about 10.5 hours.

TABLE III

SOLUTIONS OF LARGE FLAMME PROBLEMS WITH MLFMA PARALLELIZED INTO 16 PROCESSES

Frequency	12 GHz	16 GHz	20 GHz
Size	240λ	320λ	400λ
Unknowns	14,326,512	24,782,400	33,685,440
Levels	9	10	10
Smallest Cluster Size	0.235λ	0.156λ	0.195λ
BiCGStab Iterations	41	41	50
Setup Time (min.)	179	118	213
Solution Time (min.)	132	295	484

To present the accuracy of the solutions, Fig. 3 depicts the normalized bistatic radar cross section (RCS/λ^2) values in decibels (dB) for the spheres of radii 80λ, 96λ, and 110λ. To calculate the radiated fields due to the induced current on the object, we also employ the multilevel tree and calculate the radiation of clusters from the lowest level to the top of the tree structure. Then, the overall radiation of the object in a direction (θ, ϕ) is interpolated from the radiation of the clusters in the top level. In Fig. 3, analytical values obtained by Mie-series solutions are plotted as references from 150° to 180°, where 180° corresponds to the forward-scattering direction. We observe that the computational values are in agreement with the analytical curves. For more quantitative information, we define a relative error as

$$e_R = \frac{||\boldsymbol{A} - \boldsymbol{C}||_2}{||\boldsymbol{A}||_2}, \tag{11}$$

where $\boldsymbol{A}$ and $\boldsymbol{C}$ are the analytical and computational RCS values, respectively, $||.||_2$ is the l^2-norm defined as

$$||\boldsymbol{x}||_2 = \sqrt{\sum_{s=1}^{S} \left|\boldsymbol{x}[s]\right|^2}, \tag{12}$$

and S is the number of samples. For the spheres of radii 80λ, 96λ, and 110λ, the relative error is 0.045, 0.045, and 0.047, respectively, in the 150°–180° range.

Next, we present the solution of a real-life problem involving the Flamme, which is a stealth airborne target, as detailed in [24]. The nose of the target is in the x direction and it is illuminated by a plane wave propagating in the x-y plane at a 30° angle from the x axis (from $\phi = 30^\circ$) with the electric field polarized in the θ direction. As detailed in Table III, the problem is solved at 12 GHz, 16 GHz, and 20 GHz. The maximum dimension of the Flamme is 6 meters, corresponding to 240λ, 320λ, and 400λ at these frequencies, while discretizations with $\lambda/10$ mesh size lead to 14,326,512, 24,782,400, and 33,685,440 unknowns, respectively. Table III shows that the solution of the largest problem with 33,685,440

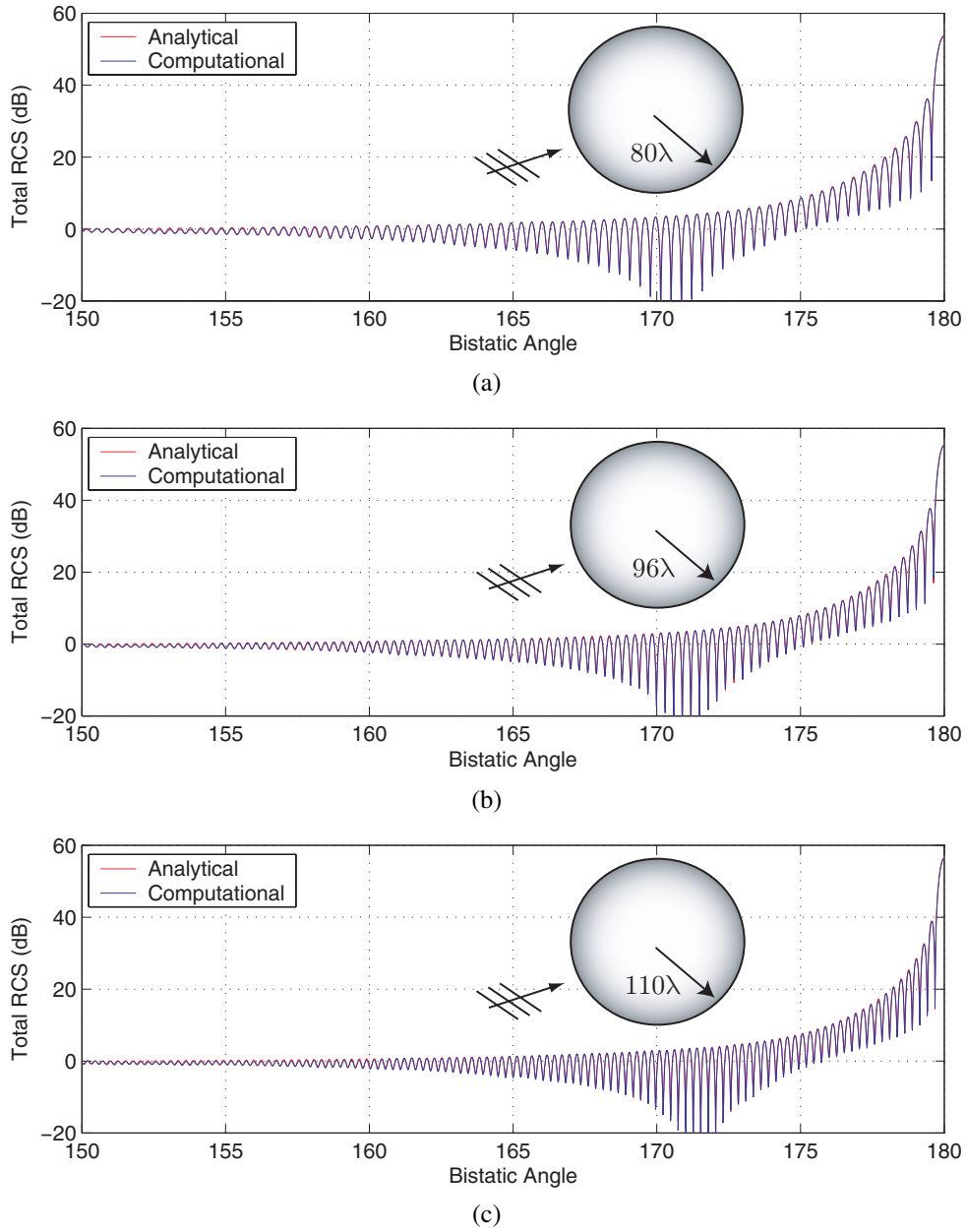

Fig. 4. Bistatic RCS (in dB) of spheres of radii (a) 80λ, (b) 96λ, and (c) 110λ from 150° to 180°, where 180° corresponds to the forward-scattering direction.

unknowns requires about 11.6 hours. Finally, Fig. 5 presents the RCS values at 12 GHz and 16 GHz on the x-y plane as a function of the bistatic angle ϕ. Both θ and ϕ polarizations are considered for the scattered fields. In the plots, 30° and 210° correspond to the back-scattering and forward-scattering directions, respectively.

V. Conclusion

In this paper, we consider fast and accurate solutions of large-scale scattering problems formulated by CFIE. Using an efficient parallel implementation of MLFMA, we are able to solve problems discretized with tens of millions of unknowns.

Acknowledgment

This work was supported by the Scientific and Technical Research Council of Turkey (TUBITAK) under Research Grant 105E172, by the Turkish Academy of Sciences in the framework of the Young Scientist Award Program (LG/TUBA-GEBIP/2002-1-12), and by contracts from ASELSAN and SSM.

References

[1] A. J. Poggio and E. K. Miller, "Integral equation solutions of three-dimensional scattering problems," in *Computer Techniques for Electromagnetics*, R. Mittra, Ed. Oxford: Pergamon Press, 1973, Chap. 4.

[2] J. R. Mautz and R. F. Harrington, "H-field, E-field, and combined field solutions for conducting bodies of revolution," *AEÜ*, vol. 32, no. 4, pp. 157–164, Apr. 1978.

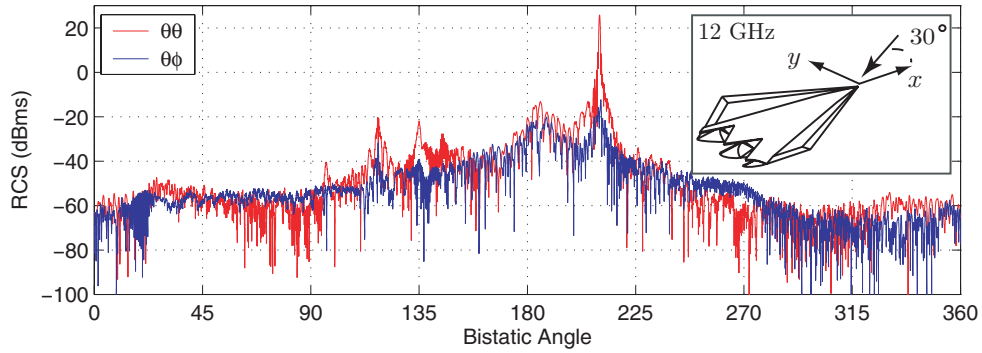

(a)

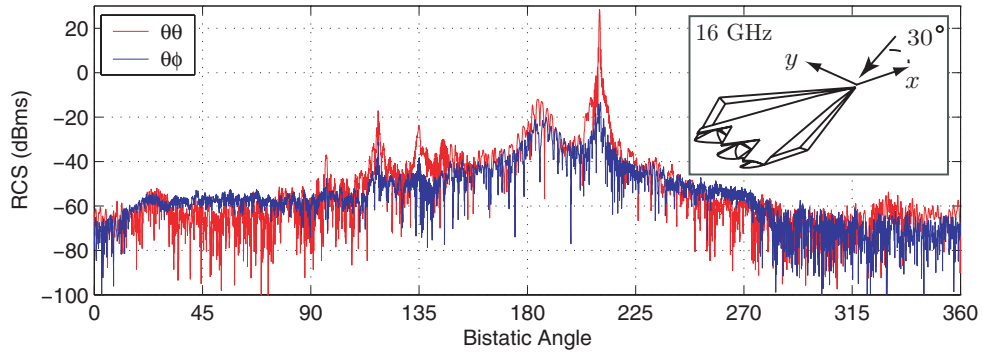

(b)

Fig. 5. Bistatic RCS (in dBm^2) of the stealth airborne target Flamme at (a) 12 GHz and (b) 16 GHz. The target is illuminated by a plane wave propagating in the x-y plane at a 30° angle from the x axis, as also depicted in the insets.

[3] D. R. Wilton and J. E. Wheeler III, "Comparison of convergence rates of the conjugate gradient method applied to various integral equation formulations," *Progress in Electromagnetics Research PIER 05*, pp. 131–158, 1991.

[4] L. Gürel and Ö. Ergül, "Comparisons of FMM implementations employing different formulations and iterative solvers," in *Proc. IEEE Antennas and Propagation Soc. Int. Symp.*, vol. 1, 2003, pp. 19–22.

[5] L. Gürel and Ö. Ergül, "Extending the applicability of the combined-field integral equation to geometries containing open surfaces," *IEEE Antennas Wireless Propagat. Lett.*, vol. 5, pp. 515–516, 2006.

[6] J. Song, C.-C. Lu, and W. C. Chew, "Multilevel fast multipole algorithm for electromagnetic scattering by large complex objects," *IEEE Trans. Antennas Propagat.*, vol. 45, no. 10, pp. 1488–1493, Oct. 1997.

[7] S. Velamparambil, W. C. Chew, and J. Song, "10 million unknowns: Is it that big?," *IEEE Ant. Propag. Mag.*, vol. 45, no. 2, pp. 43–58, Apr. 2003.

[8] M. L. Hastriter, "A study of MLFMA for large-scale scattering problems," Ph.D. thesis, University of Illinois at Urbana-Champaign, 2003.

[9] G. Sylvand, "Performance of a parallel implementation of the FMM for electromagnetics applications," *Int. J. Numer. Meth. Fluids*, vol. 43, pp. 865–879, 2003.

[10] S. Velamparambil and W. C. Chew, "Analysis and performance of a distributed memory multilevel fast multipole algorithm," *IEEE Trans. Antennas Propag.*, vol. 53, no. 8, pp. 2719–2727, Aug. 2005.

[11] Ö. Ergül and L. Gürel, "Efficient parallelization of multilevel fast multipole algorithm," in *Proc. European Conference on Antennas and Propagation (EuCAP)*, no. 350094, 2006.

[12] L. Gürel and Ö. Ergül, "Fast and accurate solutions of integral-equation formulations discretised with tens of millions of unknowns," *Electronics Lett.*, vol. 43, no. 9, pp. 499–500, Apr. 2007.

[13] S. M. Rao, D. R. Wilton, and A. W. Glisson, "Electromagnetic scattering by surfaces of arbitrary shape," *IEEE Trans. Antennas Propagat.*, vol. AP-30, no. 3, pp. 409–418, May 1982.

[14] D. A. Dunavant, "High degree efficient symmetrical Gaussian quadrature rules for the triangle," *Int. J. Numer. Meth. Eng.*, vol. 21, pp. 1129–1148, 1985.

[15] R. D. Graglia, "On the numerical integration of the linear shape functions times the 3-D Green's function or its gradient on a plane triangle," *IEEE Trans. Antennas Propagat.*, vol. 41, no. 10, pp. 1448–1455, Oct. 1993.

[16] R. E. Hodges and Y. Rahmat-Samii, "The evaluation of MFIE integrals with the use of vector triangle basis functions," *Microwave Opt. Technol. Lett.*, vol. 14, no. 1, pp. 9–14, Jan. 1997.

[17] Ö. Ergül, "Fast multipole method for the solution of electromagnetic scattering problems," M.S. thesis, Bilkent University, Ankara, Turkey, Jun. 2003.

[18] P. Y.-Oijala and M. Taskinen, "Calculation of CFIE impedance matrix elements with RWG and $\hat{\boldsymbol{n}}\times$RWG functions," *IEEE Trans. Antennas Propagat.*, vol. 51, no. 8, pp. 1837–1846, Aug. 2003.

[19] L. Gürel and Ö. Ergül, "Singularity of the magnetic-field integral equation and its extraction," *IEEE Antennas Wireless Propagat. Lett.*, vol. 4, pp. 229–232, 2005.

[20] W. C. Chew, J.-M. Jin, E. Michielssen, and J. Song, *Fast and Efficient Algorithms in Computational Electromagnetics*. Boston, MA: Artech House, 2001.

[21] S. Koc, J. M. Song, and W. C. Chew, "Error analysis for the numerical evaluation of the diagonal forms of the scalar spherical addition theorem," *SIAM J. Numer. Anal.*, vol. 36, no. 3, pp. 906–921, 1999.

[22] Ö. Ergül and L. Gürel, "Enhancing the accuracy of the interpolations and anterpolations in MLFMA," *IEEE Antennas Wireless Propagat. Lett.*, vol. 5, pp. 467–470, 2006.

[23] A. Brandt, "Multilevel computations of integral transforms and particle interactions with oscillatory kernels," *Comp. Phys. Comm.*, vol. 65, pp. 24–38, Apr. 1991.

[24] L. Gürel, H. Bağcı, J. C. Castelli, A. Cheraly, and F. Tardivel, "Validation through comparison: measurement and calculation of the bistatic radar cross section (BRCS) of a stealth target," *Radio Sci.*, vol. 38, no. 3, Jun. 2003.